

# Free energy from stationary implementation of the DFT+DMFT functional

Kristjan Haule and Turan Birol

*Department of Physics and Astronomy, Rutgers University, Piscataway, USA*

(Dated: January 29, 2015)

The stationary functional of the all-electron density functional plus dynamical mean field theory (DFT+DMFT) formalism to perform free energy calculations and structural relaxations is implemented for the first time. Here, the first order error in the density leads to a much smaller, second order error in the free energy. The method is applied to several well known correlated materials; metallic SrVO<sub>3</sub>, Mott insulating FeO, and elemental Cerium, to show that it predicts the lattice constants with very high accuracy. In Cerium, we show that our method predicts the iso-structural transition between the  $\alpha$  and  $\gamma$  phases, and resolve the long standing controversy in the driving mechanism of this transition.

PACS numbers: 71.27.+a, 71.30.+h

Prediction of the crystal structures of solids by large scale quantum mechanical simulations is one of the fundamental problems of condensed matter physics, and occupies a central place in materials design. The workhorse of the field is the Density Functional Theory (DFT) [1] at the level of Local Density Approximation (LDA) or Generalized Gradient Approximations (GGAs), which predict lattice constants of weakly correlated materials typically within  $\sim 1\%$  relative error [2].

These errors of DFT in LDA/GGA implementations are an order of magnitude larger in the so called correlated materials: For example, the lattice constant of  $\delta$ -Pu is underestimated by 11% [3] or non-magnetic FeO by 7% [4]. While GGAs and hybrid functionals can sometimes improve upon conventional LDA, these functionals many times degrade the agreement between predicted and experimentally determined bulk moduli and lattice constants, in particular in materials containing heavy elements. [2]

To account for the correlation effects, more sophisticated many body methods have been developed. Among them, one of the most successful algorithms is the dynamical mean-field theory (DMFT) [5]. It replaces the problem of describing correlation effects in a periodic lattice by a strongly interacting impurity coupled to a self-consistent bath [6]. To become material specific, DMFT was soon developed into an electronic structure tool (LDA+DMFT) [7, 8], which achieved great success in numerous correlated materials (for a review see [9]). The LDA+DMFT method has mainly been used for the calculation of spectroscopic quantities, and only a few dozens [10–30] of studies managed to compute energetics of correlated solids, and only a handful of them used exact solvers and charge self-consistency [18, 19, 24, 25, 28, 29]. This is not only because of the very high computational cost, but also because previous implementations of LDA+DMFT were not stationary, and hence it was hard to achieve precision of free energies needed for structure optimization and study of phase transitions in solids.

Here we implemented the LDA+DMFT functional,

which delivers stationary free energies at finite temperatures. This stationarity is crucial for practical implementation and precision of computed energies, since the first order error in the density  $\rho$  (or the Green's function) leads only to the much smaller second order error in the free energy, since the first order variation vanishes, i.e.,  $\delta F/\delta\rho = 0$ . This property is also crucial in calculating the forces, as stationarity of the functional ensures that only Hellmann-Feynman forces need to be computed for structural relaxation. [58]

The DFT+DMFT total energy is given by [9] :

$$E = \text{Tr}(H_0 G) + \frac{1}{2} \text{Tr}(\Sigma G) + E^H[\rho] + E^{xc}[\rho] - \Phi^{DC}[n_{loc}] + E_{nuc-nuc} \quad (1)$$

where  $H_0 = -\nabla^2 + \delta(\mathbf{r} - \mathbf{r}')V_{ext}(\mathbf{r})$ ,  $G$  is the electron Green's function,  $E^H[\rho]$  and  $E^{xc}[\rho]$  are Hartree and DFT exchange-correlation functional,  $V_{ext}$  is the electron-nuclear potential,  $E_{nuc-nuc}$  is the interaction energy of nuclei,  $\Sigma$  is the DMFT self-energy, and  $\Phi^{DC}[n_{loc}]$  is the double-counting (DC) functional. [4] Here the Migdal-Galitskii formula (MGF) is used  $E_{pot} = \frac{1}{2} \text{Tr}(\Sigma G)$  to compute the DMFT part of the potential energy.

Gordon Baym showed [31] that for certain class of approximations, which are derivable from a functional expressed in terms of closed-loop Feynman diagrams, MGF can be used instead of more complicated expression for evaluating the Luttinger-Ward Functional [32, 33]. He called such approximations conserving. While the DMFT is a conserving approximation in Baym's sense, LDA or GGA are not, as the Galitskii-Migdal formula  $\frac{1}{2} \text{Tr}(V_{xc}\rho)$  has to be replaced by the exchange-correlation functional  $E^{xc}[\rho]$ . As a result, the combination of DFT+DMFT in its charge-self consistent version is not conserving either, and consequently MGF can give different total energy than the Luttinger-Ward functional. Only the evaluation of the latter is guaranteed to give stationary free energies. We will give numerical evidence that evaluation of MGF in Eq. 1 gives different results than evaluation of the Luttinger-Ward functional, which strongly suggests

that Eq. 1 gives non-stationary total energies.

The Luttinger-Ward functional of DFT+DMFT has been well known for several years [9], but it has never been successfully implemented to compute the free energy of a solids. It has the following form

$$\Gamma[G] = \text{Tr} \log G - \text{Tr}((G_0^{-1} - G^{-1})G) + E^H[\rho] + E^{xc}[\rho] + \Phi^{DMFT}[\hat{P}G] - \Phi^{DC}[\hat{P}\rho] + E_{nuc-nuc}, \quad (2)$$

where  $G_0^{-1}(\mathbf{r}\mathbf{r}'; i\omega) = [i\omega + \mu + \nabla^2 - V_{ext}(\mathbf{r})]\delta(\mathbf{r} - \mathbf{r}')$ ,  $\Phi^{DMFT}[\hat{P}G]$  is the DMFT functional, which is the sum of all local skeleton Feynman diagrams. The projected Green's function  $\hat{P}G \equiv G_{local} = \sum_{LL'} |\phi_L\rangle \langle \phi_L| G |\phi_{L'}\rangle \langle \phi_{L'}|$  and the projected density  $\hat{P}\rho \equiv \rho_{local}$  are computed with projection to a set of localized functions  $|\phi\rangle$  centered on the "correlated" atom. The projection defines the local Green's function  $G_{local}$ , the essential variable of the DMFT.

The variation of functional  $\Gamma[G]$  with respect to  $G$  ( $\delta\Gamma[G]/\delta G$ ) gives,

$$G^{-1} - G_0^{-1} + (V_H + V_{xc})\delta(\mathbf{r} - \mathbf{r}')\delta(\tau - \tau') + \hat{P} \frac{\delta\Phi^{DMFT}[G_{local}]}{\delta G_{local}} - \hat{P} \frac{\delta\Phi^{DC}[\rho_{local}]}{\delta \rho_{local}} \delta(\mathbf{r} - \mathbf{r}')\delta(\tau - \tau') = 0, \quad (3)$$

which vanishes, since it is equal to the Dyson equation that determines self-consistent  $G$ , hence the functional is stationary.

The value of the functional  $\Gamma$  at the self-consistently determined  $G$  delivers the free energy of the system [31]. We evaluate it by inserting  $G_0^{-1} - G^{-1}$  from Eq. 3 into Eq. 2 to obtain

$$F = E_{nuc-nuc} - \text{Tr}((V_H + V_{xc})\rho) + E^H[\rho] + E^{xc}[\rho] + \text{Tr} \log G - \text{Tr} \log G_{loc} + F_{imp} + \text{Tr}(V_{dc}\rho_{loc}) - \Phi^{DC}[\rho_{loc}] + \mu N, \quad (4)$$

where we denoted  $V_{dc} \equiv \delta\Phi^{DC}[\rho_{local}]/\delta\rho_{local}$  and  $F_{imp}$  is the free energy of the impurity problem, i.e.,  $F_{imp} = \text{Tr} \log G_{loc} - \text{Tr}(\Sigma G_{loc}) + \Phi^{DMFT}[G_{loc}]$ . [4] Here we also use the fact the solution of the auxiliary impurity problem delivers the exact local Green's function, i.e.,  $\Sigma = \delta\Phi^{DMFT}[G_{local}]/\delta G_{local}$ , and we added  $\mu N$  because we work at constant electron number.

The crucial point is that the continuous time quantum Monte Carlo method (CTQMC) [34, 35] solves the quantum impurity model (QIM) numerically exactly, hence, we can compute very precisely the impurity internal energy as well as the free energy  $F_{imp}$  of this model. At high enough temperature,  $F_{imp}$  can be directly read-off from the probability for the perturbation order  $k$ , which we call  $P_k$ , and is computed by  $P_k = Z_k/Z$  (where  $Z_k$  is the partition function with  $k$ -kinks), hence  $Z = Z_{atom}/P_0$ ,

where  $Z_{atom}$  can be directly computed from atomic energies, and  $P_0$  is the probability for no kinks on the impurity. Finally,  $Z = \exp(-F_{imp}/T)$ , giving directly

$$F_{imp} = -T(\log(Z_{atom}) - \log(P_0)). \quad (5)$$

When the temperature is low,  $P_0$  becomes exponentially small, and we can no longer determine  $Z$  to high enough precision in this way. However, we can compute very precisely the internal energy of the impurity at arbitrary temperature. The internal energy of QIM  $E_{imp}$  is given by

$$E_{imp} = \text{Tr}((\Delta + \varepsilon_{imp} - \omega_n \frac{d\Delta}{d\omega_n})G_{imp}) + E_{imp-pot}, \quad (6)$$

which follows directly from the thermodynamic average of QIM Hamiltonian. Here the hybridization  $\Delta$  and impurity levels  $\varepsilon_{imp}$  are determined from the local green's function by the standard DMFT self-consistency condition  $G_{local}^{-1} = i\omega_n - \varepsilon_{imp} - \Sigma - \Delta$ , and  $E_{imp-pot} = \frac{1}{2}\text{Tr}(\Sigma G_{imp})$ . These quantities can be computed very precisely by CTQMC using the following tricks: i)  $\text{Tr}(\Delta G_{imp})$  is computed from the average perturbation order  $\langle k \rangle$  of CTQMC, and takes the form  $\text{Tr}(\Delta G_{imp}) = \langle k \rangle / T$ , where  $T$  is temperature [34]; ii)  $E_{imp-pot}$  is computed from the energies of atomic state of QIM  $E_m^{atom}$  and their probabilities  $P_m$  by  $E_{imp-pot} = \sum_m P_m E_m^{atom} - \text{Tr}(\varepsilon_{imp} n_{imp})$  [34], which delivers much more precise interaction energy than obtained by MGF; ii) We spline  $\Delta(\omega_n)$  in Matsubara points and determine its derivative  $d\Delta/d\omega_n$ , and then carry out Matsubara sum by subtracting out the leading high-frequency tails by formula  $A/((i\omega - \varepsilon_1)(i\omega - \varepsilon_2))$ , which has an analytic sum of  $A(f(\varepsilon_1) - f(\varepsilon_2))/(\varepsilon_1 - \varepsilon_2)$ . Because probabilities  $P_m$  and perturbation order  $\langle k \rangle$  are known to very high precision in CTQMC, the impurity internal energy can easily be computed with precision of a fraction of a meV.

To compute precise impurity free energy  $F_{imp}$  at lower temperature, we first converge DFT+DMFT equations to high accuracy at low temperature. Using converged impurity hybridization  $\Delta(i\omega_n)$ , we raise the temperature of the impurity (keeping  $\Delta$  fixed) to  $T_>$ , so that  $P_0$  is of the order of  $10^{-5}$  or higher, and obtain reliable  $F_{imp}$  using Eq. 5, and entropy  $S_{imp}$  at this higher temperature  $S_> = (E_{imp}(T_>) - F_{imp}(T_>))/T_>$ . Next, we evaluate impurity internal energy for several inverse temperatures  $\beta = 1/T$ , and than we use standard thermodynamic relations to obtain entropy at lower temperature  $T$  by

$$S(T) = S_> - \frac{E_{imp}(T_>)}{T_>} + \frac{E_{imp}(T)}{T} - \int_{1/T_>}^{1/T} E_{imp}(\beta) d\beta(\tau)$$

where  $\beta = 1/T$ . This formula is obtained integrating by parts the standard formula  $S = \int c_v/T dT$  and  $c_v = dE/dT$ . We hence obtain  $S_{imp}$  and  $F_{imp} = E_{imp} - TS_{imp}$  at lower  $T$  which can be inserted into Eq. 4. The rest

of the terms in Eq. 4 are relatively straightforward to evaluate, however, for a high precision implementation one needs to combine the terms that largely cancel and evaluate them together [4].

Previous implementations of free energy within LDA+DMFT [25, 27, 36] were based on i) evaluating the total energy Eq. 1 at range of temperatures, and integrating resulting specific heat [36], and ii) the coupling constant integration [25, 27], where total energy of the solid is needed for a range of coulomb repulsion's  $U$  and is than integrated over  $U$ . In both approaches, the self-consistent LDA+DMFT solution is needed for many values of the parameters (either  $U$  or  $T$ ) to evaluate  $F$ . In our method, a single LDA+DMFT calculation for solid is needed, which makes the method much more efficient. Furthermore, current implementation of the free energy is stationary, hence higher precision of  $F$  is achieved.

To test the implementation of the LDA+DMFT functional, we computed the volume dependence of the free energy for three well studied correlated materials: a metallic early transition metal oxide with perovskite structure  $\text{SrVO}_3$ , a Mott insulating transition metal oxide  $\text{FeO}$  in its rock salt structure, and the lanthanide elemental metal, Cerium, in its face centered cubic structure, which undergoes a first order iso-structural transition.

We used the implementation of LDA+DMFT of Ref.37, which is based on the Wien2K package [38], and LDA in combination with nominal double-counting [37, 39, 40]. More technical details are given in the supplementary information.

In Fig. 1(a) we show the energy  $E(V)$ , and  $F(V)$  for  $\text{SrVO}_3$  at  $T = 230\text{K}$ , computed with Eq. 1, and Eq. 4, respectively. The minima of  $E(V)$  and  $F(V)$  are achieved at  $55.71\text{\AA}^3$  and  $55.51\text{\AA}^3$ . The experimentally determined volume is  $V_{exp} = 56.53\text{\AA}^3$  [42]. The LDA+DMFT hence slightly underestimates the equilibrium volume (1.8%), which gives 0.6% error in lattice constant. This is well within the standard error of best DFT functionals for weakly correlated materials.

The metallic nature of  $\text{SrVO}_3$ , with moderate mass enhancements  $m^*/m_{band} \approx 2$  [4], leads to very small DMFT corrections in crystal structure [4]. Note that energy minimization leads to slightly larger volume than free energy minimization, contrary to expectations. This is because energy is computed from non-stationary Eq. 1, while free energy is obtained from the stationary expression Eq. 4. The latter is hence more trustworthy, and should be considered best LDA+DMFT result. This is also clear from pressure versus volume diagram in Fig. 1(b), where  $-dF/dV$  agrees more favorably with the experiment than  $-dE/dV$  obtained by MGF.

In Fig. 1(c), we show the impurity entropy obtained by Eq. 7 for two representative volumes. In this itinerant system with very large hybridization, we do not

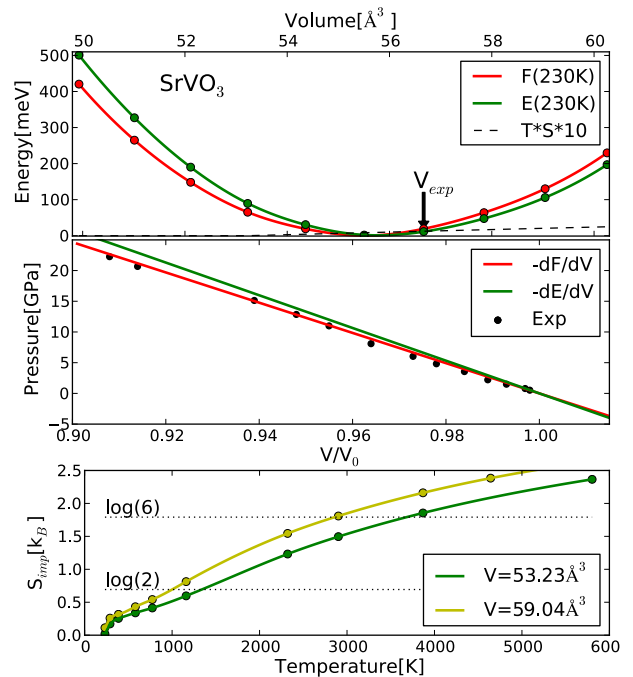


FIG. 1: (Color online): a)  $E(V)$  and  $F(V)$  for  $\text{SrVO}_3$  at  $T = 230\text{K}$  from Eq. 1 and 4, respectively. Entropy term  $TS_{imp}(V)$  is very small. (b) theoretical and experimental [41]  $p(V)$ . Good agreement between theoretical  $-dF/dV$  and experiment is found. (c) Impurity Entropy Eq. 7 for representative volumes. To obtain  $S_{imp}$ , temperature is varied in the impurity problem only, and not in the LDA+DMFT problem of the solid.

notice a temperature scale at which  $t_{2g}$  shell is degenerate ( $\log(6)$ ) nor the scale of the lowest order Kramers doublet ( $\log(2)$ ), but we notice the Fermi liquid scale in the steep downturn of  $S(T)$  at  $T \approx 350\text{K}$ .

Fig. 2(a) shows  $E(V)$  and  $F(V)$  for paramagnetic Mott insulating  $\text{FeO}$  at  $300\text{K}$ , above its antiferromagnetic ordering temperature. The equilibrium volume of  $E$  and  $F$  is  $20.28\text{\AA}^3$  and  $20.24\text{\AA}^3$ , while the experimental volume is  $20.34\text{\AA}^3$ . The lattice constant is thus underestimated for only 0.10% and 0.16%, respectively. In comparison, all standard DFT functionals severely underestimate  $\text{FeO}$  lattice constant, for example PBE-sol, PBE, and LDA for 5.2%, 5.0%, and 7.7%, respectively.

In Fig. 2(b) we show  $P(V)$  diagram and its excellent agreement with experiment. Fig. 2(c) shows impurity entropy  $S_{imp}(T)$  for a few volumes. In contrast to metallic  $\text{SrVO}_3$ , here we clearly see an extended plateau of  $S_{imp}(T) = \log(6) * k_B$  around  $1000\text{K}$ , which signals complete degeneracy of the  $t_{2g}$  shell, and its slight decrease at  $300\text{K}$  in proximity to the AFM state.

The iso-structural transitions of Cerium attracted a lot of experimental and theoretical effort, but its theoretical understanding is still controversial. On the basis of LDA+DMFT calculation McMahan *et.al* [11] proposed that the total energy exhibits a double-minimum

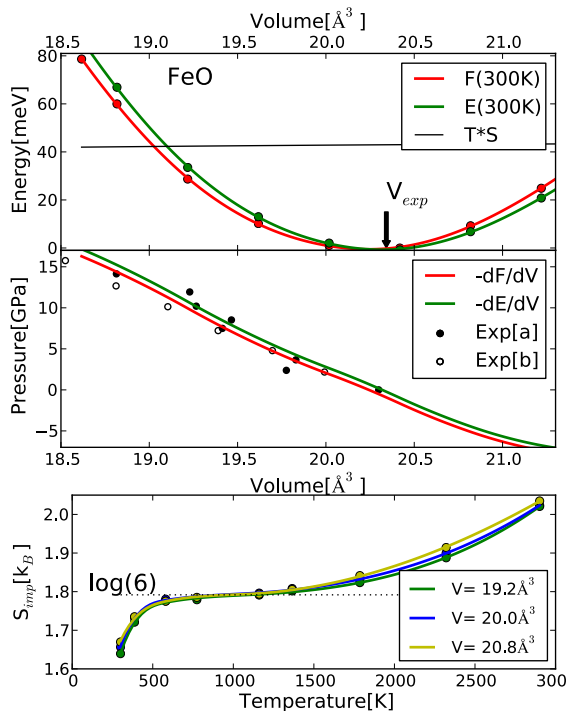


FIG. 2: (Color online): a)  $E(V)$  and  $F(V)$  for FeO from Eq. 1 and 4, respectively. Entropy term  $TS_{imp}(V)$  is large but almost constant. (b) theoretical and experimental  $p(V)$ . Filled and empty circles are from Refs. 43 and 44, respectively. (c) Impurity entropy Eq. 7 for representative volumes. The degeneracy of the  $t_{2g}$  shell above 1000K is apparent.

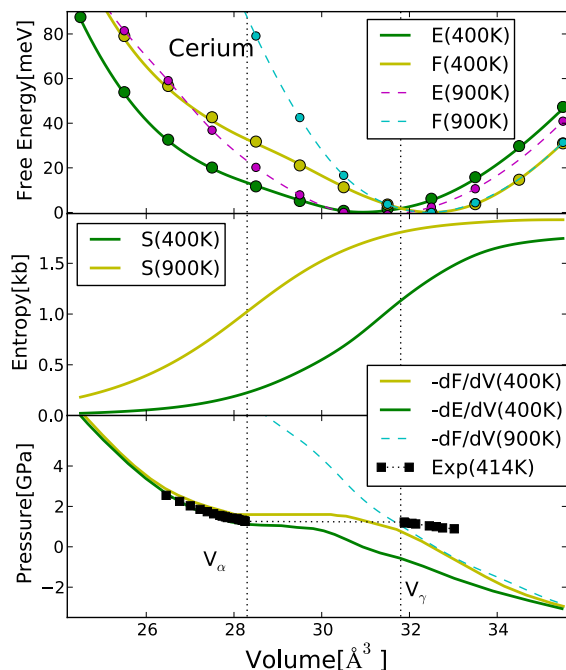


FIG. 3: (Color online): a)  $E(V)$  and  $F(V)$  for elemental Cerium from Eq. 1 and 4, respectively. Data are presented for  $T=400$  and  $900$  K. (b) Entropy  $S_{imp}(V)$  is large and changes dramatically across the transition. (c) theoretical and experimental [45]  $p(V)$  diagram.

shape, concomitant with the appearance of the quasiparticle peak at temperature as high as 1500 K, signaling the first order transition. Using different implementation of the same method, Amadon *et.al* [27, 46] proposed that the transition is entropy driven, and that the total energy is featureless with the minimum corresponding to low volume  $\alpha$ -phase. Only the addition of the entropy term moves the minimum to the larger volume of  $\gamma$ -phase. In this picture the transition at low temperatures, where the entropy becomes small and cannot drive the transition, is intrinsically absent. Yet another proposal was recently put forward on the basis of LDA+Gutzwiller calculations [47, 48], in which the transition is present even at zero temperature, but the transition occurs at negative pressure. The transition is thus detectable even in the total energy, in the absence of entropy, and becomes second order at  $T = 0$ . In the same method, the finite temperature transition is first order, and the double-minimum shape of free energy becomes most pronounced at very high temperature (1500 K) [48].

Our LDA+DMFT results for Ce are plotted in Fig. 3. The total energy curve at 400 K clearly shows a region of very flat shape in the region between the  $\alpha$ - $\gamma$  volume. Indeed the derivative of the energy  $-dE/dV$  displayed in Fig. 3(c) shows a clear region of zero slope around 1 GPa. This is consistent with results of Lanata *et.al.* [47] finding very similar zero slope of  $-dE/dV$  at zero temperature, but is inconsistent with Ref. 27, which finds no feature in total energy. It is also inconsistent with McMahan *et.al* [11] showing clear double-peak in total energy. On the other hand, the addition of entropy substantially increase the region of soft volume, as suggested by Amadon *et.al* [46]. Indeed the change of the entropy between the two phases is of the order of  $0.9k_B$ , which is consistent with experimental estimations of 30 meV at 400K [49]. The physical mechanism behind this large entropy change and unusual volume dependence of energy is in very fast variation of coherence temperature, as suggested in Refs. [11, 46], and conjectured in Kondo volume collapse theory [50]. The phase transition in our calculation occurs around 1.6 GPa, which is not far from experimentally determined critical pressure of 1.25 GPa at  $T = 400$  K. The free energy barrier in our calculation is however extremely small, and no clear double peak of  $F(V)$  or negative slope of  $-dF/dV$  can be detected within our 1 meV precision of energies. This is similar to results of Ref. 48 at 400 K, but different from Ref. 11. While the start of the transition region in  $\alpha$ -phase is in good agreement with experiment, the  $\gamma$ -phase volume is underestimated in our calculation. We believe that the addition of phonon entropy is needed to further increase the transition region, and establish larger free energy barrier between the two phases. Experimentally, above 460 K the  $\alpha - \gamma$  phase transition ends with the finite temperature critical point. Our calculation at high temperature 900 K shows that the signature of the phase

transition in  $F(V)$  and  $E(V)$  disappears, which is different than predicted by Gutzwiller method [48], where the largest free energy barrier is found at these elevated temperatures, but qualitatively consistent with Ref. 11 .

In summary, we successfully implemented the stationary formula for the free energy of DFT+DMFT method. On the example of  $\text{SrVO}_3$ ,  $\text{FeO}$  and  $\text{Ce}$  metal we demonstrated that the method successfully predicts lattice volumes in correlated solids, which are difficult for standard DFT functionals. We also resolved controversy in the mechanism of the  $\alpha$ - $\gamma$  transition in Cerium.

This work was supported Simons foundation under project "Many Electron Problem", and by NSF-DMR 1405303. T.B. was supported by the Rutgers Center for Materials Theory. This research used resources of the Oak Ridge Leadership Computing Facility at the Oak Ridge National Laboratory, which is supported by the Office of Science of the US Department of Energy under Contract No. DE-AC05-00OR22725.

- 
- [1] P. Hohenberg and W. Kohn, Phys. Rev. **136**, B864 (1964), URL <http://link.aps.org/doi/10.1103/PhysRev.136.B864>.
- [2] A. E. Mattsson, R. Armiento, J. Paier, G. Kresse, J. M. Wills, and T. R. Mattsson, The Journal of Chemical Physics **128**, 084714 (2008), URL <http://scitation.aip.org/content/aip/journal/jcp/128/8/10.1063/1.2835596>.
- [3] S. Y. Savrasov, G. Kotliar, and E. Abrahams, Nature **410**, 793 (2001), URL <http://dx.doi.org/10.1038/35071035>.
- [4] *For more information see the supplementary information.*
- [5] A. Georges and G. Kotliar, Phys. Rev. B **45**, 6479 (1992), URL <http://link.aps.org/doi/10.1103/PhysRevB.45.6479>.
- [6] A. Georges, G. Kotliar, W. Krauth, and M. J. Rozenberg, Rev. Mod. Phys. **68**, 13 (1996), URL <http://link.aps.org/doi/10.1103/RevModPhys.68.13>.
- [7] V. I. Anisimov, A. I. Poteryaev, M. A. Korotin, A. O. Anokhin, and G. Kotliar, Journal of Physics: Condensed Matter **9**, 7359 (1997), URL <http://stacks.iop.org/0953-8984/9/i=35/a=010>.
- [8] A. I. Lichtenstein and M. I. Katsnelson, Physical Review B **57**, 6884 (1998), URL <http://dx.doi.org/10.1103/PhysRevB.57.6884>.
- [9] G. Kotliar, S. Y. Savrasov, K. Haule, V. S. Oudovenko, O. Parcollet, and C. A. Marianetti, Rev. Mod. Phys. **78**, 865 (2006), URL <http://link.aps.org/doi/10.1103/RevModPhys.78.865>.
- [10] S. Y. Savrasov, G. Kotliar, and E. Abrahams, Nature **410**, 793 (2001).
- [11] K. Held, A. K. McMahan, and R. T. Scalettar, Phys. Rev. Lett. **87**, 276404 (2001), URL <http://link.aps.org/doi/10.1103/PhysRevLett.87.276404>.
- [12] A. K. McMahan, K. Held, and R. T. Scalettar, Phys. Rev. B **67**, 075108 (2003), URL <http://link.aps.org/doi/10.1103/PhysRevB.67.075108>.
- [13] B. Amadon, S. Biermann, A. Georges, and F. Aryasetiawan, Phys. Rev. Lett. **96**, 066402 (2006), URL <http://link.aps.org/doi/10.1103/PhysRevLett.96.066402>.
- [14] S. Y. Savrasov, K. Haule, and G. Kotliar, Phys. Rev. Lett. **96**, 036404 (2006), URL <http://link.aps.org/doi/10.1103/PhysRevLett.96.036404>.
- [15] L. V. Pourovskii, B. Amadon, S. Biermann, and A. Georges, Phys. Rev. B **76**, 235101 (2007), URL <http://link.aps.org/doi/10.1103/PhysRevB.76.235101>.
- [16] I. Leonov, N. Binggeli, D. Korotin, V. I. Anisimov, N. Stojić, and D. Vollhardt, Phys. Rev. Lett. **101**, 096405 (2008), URL <http://link.aps.org/doi/10.1103/PhysRevLett.101.096405>.
- [17] I. Di Marco, J. Minár, S. Chadov, M. I. Katsnelson, H. Ebert, and A. I. Lichtenstein, Phys. Rev. B **79**, 115111 (2009), URL <http://link.aps.org/doi/10.1103/PhysRevB.79.115111>.
- [18] M. Aichhorn, L. Pourovskii, and A. Georges, Phys. Rev. B **84**, 054529 (2011), URL <http://link.aps.org/doi/10.1103/PhysRevB.84.054529>.
- [19] G. Lee, H. S. Ji, Y. Kim, C. Kim, K. Haule, G. Kotliar, B. Lee, S. Khim, K. H. Kim, K. S. Kim, et al., Phys. Rev. Lett. **109**, 177001 (2012), URL <http://link.aps.org/doi/10.1103/PhysRevLett.109.177001>.
- [20] B. Amadon, Journal of Physics: Condensed Matter **24**, 075604 (2012), URL <http://stacks.iop.org/0953-8984/24/i=7/a=075604>.
- [21] I. Leonov, A. I. Poteryaev, V. I. Anisimov, and D. Vollhardt, Phys. Rev. B **85**, 020401 (2012), URL <http://link.aps.org/doi/10.1103/PhysRevB.85.020401>.
- [22] M. S. Litsarev, I. Di Marco, P. Thunström, and O. Eriksson, Phys. Rev. B **86**, 115116 (2012), URL <http://link.aps.org/doi/10.1103/PhysRevB.86.115116>.
- [23] O. Grns, I. D. Marco, P. Thunstrm, L. Nordstrm, O. Eriksson, T. Bjrkman, and J. Wills, Computational Materials Science **55**, 295 (2012), ISSN 0927-0256, URL <http://www.sciencedirect.com/science/article/pii/S092702561100646X>.
- [24] D. Grieger, C. Piefke, O. E. Peil, and F. Lechermann, Phys. Rev. B **86**, 155121 (2012), URL <http://link.aps.org/doi/10.1103/PhysRevB.86.155121>.
- [25] L. V. Pourovskii, T. Miyake, S. I. Simak, A. V. Ruban, L. Dubrovinsky, and I. A. Abrikosov, Phys. Rev. B **87**, 115130 (2013), URL <http://link.aps.org/doi/10.1103/PhysRevB.87.115130>.
- [26] I. Leonov, V. I. Anisimov, and D. Vollhardt, Phys. Rev. Lett. **112**, 146401 (2014), URL <http://link.aps.org/doi/10.1103/PhysRevLett.112.146401>.
- [27] J. Bieder and B. Amadon, Phys. Rev. B **89**, 195132 (2014), URL <http://link.aps.org/doi/10.1103/PhysRevB.89.195132>.
- [28] S. Mandal, R. E. Cohen, and K. Haule, Phys. Rev. B **89**, 220502 (2014), URL <http://link.aps.org/doi/10.1103/PhysRevB.89.220502>.
- [29] H. Park, A. J. Millis, and C. A. Marianetti, Phys. Rev. B **89**, 245133 (2014), URL <http://link.aps.org/doi/10.1103/PhysRevB.89.245133>.
- [30] H. Park, A. J. Millis, and C. A. Marianetti, Phys. Rev. B **90**, 235103 (2014), URL <http://link.aps.org/doi/10.1103/PhysRevB.90.235103>.
- [31] G. Baym, Phys. Rev. **127**, 1391 (1962), URL <http://link.aps.org/doi/10.1103/PhysRev.127.1391>.
- [32] J. M. Luttinger and J. C. Ward, Phys. Rev. **118**, 1417 (1960), URL <http://link.aps.org/doi/10.1103/>

- PhysRev.118.1417.
- [33] G. Baym and L. P. Kadanoff, Phys. Rev. **124**, 287 (1961), URL <http://link.aps.org/doi/10.1103/PhysRev.124.287>.
- [34] K. Haule, Phys. Rev. B **75**, 155113 (2007), URL <http://link.aps.org/doi/10.1103/PhysRevB.75.155113>.
- [35] P. Werner, A. Comanac, L. de' Medici, M. Troyer, and A. J. Millis, Phys. Rev. Lett. **97**, 076405 (2006), URL <http://link.aps.org/doi/10.1103/PhysRevLett.97.076405>.
- [36] K. Held, A. K. McMahan, and R. T. Scalettar, Phys. Rev. Lett. **87**, 276404 (2001), URL <http://link.aps.org/doi/10.1103/PhysRevLett.87.276404>.
- [37] K. Haule, C.-H. Yee, and K. Kim, Phys. Rev. B **81**, 195107 (2010), URL <http://link.aps.org/doi/10.1103/PhysRevB.81.195107>.
- [38] P. Blaha, K. Schwarz, G. K. H. Madsen, D. Kvasnicka, and J. Luitz, *WIEN2K, An Augmented Plane Wave + Local Orbitals Program for Calculating Crystal Properties* (Karlheinz Schwarz, Techn. Universität Wien, Austria, 2001).
- [39] K. Haule, T. Birol, and G. Kotliar, Phys. Rev. B **90**, 075136 (2014), URL <http://link.aps.org/doi/10.1103/PhysRevB.90.075136>.
- [40] K. Haule, eprint arXiv:1501.03438v1 (2015), URL <http://arxiv.org/abs/1501.03438>.
- [41] R. Hrubciak, Ph.D. thesis, Florida International University (2012), URL <http://digitalcommons.fiu.edu/cgi/viewcontent.cgi?article=1802&context=etd>.
- [42] M. Goodenough, J. B. and Longo, SpringerMaterials - The Landolt-Brnstein Database **4a** (1970), URL [http://dx.doi.org/10.1007/10201420\\_50](http://dx.doi.org/10.1007/10201420_50).
- [43] T. Yagi, T. Suzuki, and S.-I. Akimoto, Journal of Geophysical Research: Solid Earth **90**, 8784 (1985), ISSN 2156-2202, URL <http://dx.doi.org/10.1029/JB090iB10p08784>.
- [44] R. L. Clendenen and H. G. Drickamer, The Journal of Chemical Physics **44**, 4223 (1966), URL <http://scitation.aip.org/content/aip/journal/jcp/44/11/10.1063/1.1726610>.
- [45] M. J. Lipp, D. Jackson, H. Cynn, C. Aracne, W. J. Evans, and A. K. McMahan, Phys. Rev. Lett. **101**, 165703 (2008), URL <http://link.aps.org/doi/10.1103/PhysRevLett.101.165703>.
- [46] B. Amadon, S. Biermann, A. Georges, and F. Aryasetiawan, Phys. Rev. Lett. **96**, 066402 (2006), URL <http://link.aps.org/doi/10.1103/PhysRevLett.96.066402>.
- [47] N. Lanatà, Y.-X. Yao, C.-Z. Wang, K.-M. Ho, J. Schmalian, K. Haule, and G. Kotliar, Phys. Rev. Lett. **111**, 196801 (2013), URL <http://link.aps.org/doi/10.1103/PhysRevLett.111.196801>.
- [48] N. Lanatà, Y.-X. Yao, C.-Z. Wang, K.-M. Ho, and G. Kotliar, Phys. Rev. B **90**, 161104 (2014), URL <http://link.aps.org/doi/10.1103/PhysRevB.90.161104>.
- [49] F. Decremps, L. Belhadi, D. L. Farber, K. T. Moore, F. Occelli, M. Gauthier, A. Polian, D. Antonangeli, C. M. Aracne-Ruddle, and B. Amadon, Phys. Rev. Lett. **106**, 065701 (2011), URL <http://link.aps.org/doi/10.1103/PhysRevLett.106.065701>.
- [50] J. W. Allen and L. Z. Liu, Phys. Rev. B **46**, 5047 (1992), URL <http://link.aps.org/doi/10.1103/PhysRevB.46.5047>.
- [51] K. Ohta, R. E. Cohen, K. Hirose, K. Haule, K. Shimizu, and Y. Ohishi, Phys. Rev. Lett. **108**, 026403 (2012), URL <http://link.aps.org/doi/10.1103/PhysRevLett.108.026403>.
- [52] A. McMahan, C. Huscroft, R. Scalettar, and E. Pollock, Journal of Computer-Aided Materials Design **5**, 131 (1998), ISSN 0928-1045, URL <http://dx.doi.org/10.1023/A:3A1008698422183>.
- [53] M. Weinert, E. Wimmer, and A. J. Freeman, Phys. Rev. B **26**, 4571 (1982), URL <http://link.aps.org/doi/10.1103/PhysRevB.26.4571>.
- [54] E. Gull, A. J. Millis, A. I. Lichtenstein, A. N. Rubtsov, M. Troyer, and P. Werner, Rev. Mod. Phys. **83**, 349 (2011), URL <http://link.aps.org/doi/10.1103/RevModPhys.83.349>.
- [55] J. P. Perdew, K. Burke, and M. Ernzerhof, Phys. Rev. Lett. **77**, 3865 (1996).
- [56] J. P. Perdew, A. Ruzsinszky, G. I. Csonka, O. A. Vydrov, G. E. Scuseria, L. A. Constantin, X. Zhou, and K. Burke, Phys. Rev. Lett. **100**, 136406 (2008), URL <http://link.aps.org/doi/10.1103/PhysRevLett.100.136406>.
- [57] M. Takizawa, M. Minohara, H. Kumigashira, D. Toyota, M. Oshima, H. Wadati, T. Yoshida, A. Fujimori, M. Lippmaa, M. Kawasaki, et al., Phys. Rev. B **80**, 235104 (2009), URL <http://link.aps.org/doi/10.1103/PhysRevB.80.235104>.
- [58] Note that Pulay forces appear when incomplete basis set is used.

**SUPPLEMENTARY INFORMATION: FREE ENERGY FROM STATIONARY IMPLEMENTATION OF THE DFT+DMFT FUNCTIONAL**

**TECHNICAL DESCRIPTION OF COMPUTATIONAL DETAILS**

We used the implementation of LDA+DMFT of Ref.37, which is based on Wien2K package [38]. The exchange-correlation functional  $E_{xc}$  of LDA was utilized, in combination with nominal double-counting (DC) [37, 39], which was shown to be closest to the exact form of DC [40]. We checked (on the example of Cerium) that the exact-DC gives very similar free energy, as expected for a stationary functional. The convergence of LDA+DMFT results is much faster using nominal DC, hence most of results in this publication are obtained by this simplification.

The impurity model is solved using the hybridization expansion version of the numerically exact continuous time QMC method [34, 35]. Of the order of 300 LDA and 30 DMFT iterations were required for precision of 1 meV per formula unit, and between  $10^9 - 10^{10}$  Monte Carlo moves were accepted per impurity iteration for precise enough impurity solution. The resources of Titan supercomputer were used.

To construct the projector, the atomic-like local orbitals are used  $\langle \mathbf{r} | \phi_{lm} \rangle = \frac{u_l(r)}{r} Y_{lm}(\hat{\mathbf{r}})$ . The radial part of the local orbital  $u_l(r)$  is the solution of the scalar relativistic Dirac equation inside the muffin-tin sphere, linearized at the Fermi level. The muffin-tin spheres are set to touch at the lowest volume. We tested a few other forms of the projectors defined in Ref. 37. The stationary  $F(V)$  is quite insensitive to the precise choice of projector, however,  $E(V)$  changes much more.

For SrVO<sub>3</sub> calculations, we treated dynamically all five

$3d$  orbitals of Vanadium. The muffin-tin radius of Vanadium was set to  $R_{mt} = 1.83 a_B$ , and  $U = 10$  eV was used, which was previously shown to give good spectra [39, 40] for this localized orbital (see spectra below). The Yukawa form of screening interaction than gives  $J \approx 1$  eV (see note below). Brillouin zone integrations were done over  $15 \times 15 \times 15$  k-point in the whole zone in the self-consistent calculations, and for calculation of the impurity entropy, the hybridization is computed on more precise  $36 \times 36 \times 36$  k-points mesh. We mention in passing that impurity entropy is very sensitive to the precise frequency dependence of the hybridization, and requires very dense momentum mesh.

For FeO, all five  $3d$  orbitals are treated by DMFT and the muffin-tin radius of iron is set to  $R_{mt} = 2.11 a_B$ , and the Coulomb repulsion to previously determined  $U = 8$  eV [51], which requires  $J \approx 1$  eV in Yukawa form. In Ce metal, all seven  $4f$  orbitals are treated by DMFT and the muffin-tin sphere is  $R_{mt} = 2.5 a_B$ , the k-point mesh is  $21 \times 21 \times 21$ , and the Coulomb  $U = 6$  eV [27, 46, 52], leads to  $J = 0.72$  eV in Yukawa form. The spin-orbit coupling is included in Cerium, but neglected in SrVO<sub>3</sub> and FeO.

**DETAILS ON EVALUATION OF LDA+DMFT FUNCTIONAL**

Here we explain how we evaluate the total energy Eq.1 and the free energy Eq.4 of the main text.

For total energy Eq.1, we group the terms in the following way

$$E = \text{Tr}((-\nabla^2 + V_{ext} + V_H + V_{xc})G) - \text{Tr}((V_H + V_{xc})\rho) + E^H[\rho] + E^{xc}[\rho] + E_{nuc-nuc} + \frac{1}{2}\text{Tr}(\Sigma G) - \Phi^{DC}[\rho_{loc}] \quad (8)$$

We then split the energy into three terms  $E = E_1 + E_2 + E_3$ , where the first two parts  $E_1, E_2$  are computed using the Green's function of the solid, and the third  $E_3$  using the impurity Green's function.

The first five terms in Eq. 8 look similar to the standard DFT energy functional, except that the Green's function  $G$  here is the self-consistent LDA+DMFT Green's function. We first solve the eigenvalue problem for Kohn-Sham states  $(-\nabla^2 + V_{ext} + V_H + V_{xc})\psi_{ik} = \varepsilon_{ik}^{DFT}\psi_{ik}$ , where  $\varepsilon_{ik}^{DFT}$  are DFT-like energies, computed

on LDA+DMFT charge. We then evaluate

$$E_1 = \text{Tr}(\varepsilon^{DFT} G) \quad (9)$$

and

$$E_2 = -\text{Tr}((V_H + V_{xc})\rho) + E^H[\rho] + E^{xc}[\rho] + E_{nu-nu} \quad (10)$$

Both  $E_1$  and  $E_2$  are computed using Green's function  $G$  and density  $\rho$  of the solid in the same way as the standard DFT total energy is implemented [53].

The last two terms of Eq. 8 can be computed either from the local Green's function  $\hat{P}G$  or from the impu-

rity Green's function  $G_{imp}$ . Once the self-consistency is reached, the two are of course equal. We choose to evaluate the second term on the impurity  $G_{imp}$

$$E_3 = \frac{1}{2} \text{Tr}(\Sigma_{imp} G_{imp}) - \Phi^{DC}[\rho_{imp}] \quad (11)$$

However, we never actually use Migdal-Galitskii formula, because it is numerically much less stable than computing

the potential energy from the impurity probabilities, i.e.,

$$\frac{1}{2} \text{Tr}(\Sigma_{imp} G_{imp}) = \sum_m P_m E_m^{atom} - \text{Tr}(\varepsilon_{imp} n_{imp})$$

The free energy functional  $\Gamma[G]$  (Eq. 2 of the main text) is

$$\Gamma[G] = \text{Tr} \log G - \text{Tr} \log((G_0^{-1} - G^{-1})G) + E^H[\rho] + E^{xc}[\rho] + \Phi^{DMFT}[G_{loc}] - \Phi^{DC}[\rho_{loc}] + E_{nuc-nuc}. \quad (12)$$

First, we extremize it ( $\delta\Gamma[G]/\delta G = 0$ ) to obtain the Dyson equation

$$G^{-1} - G_0^{-1} + V_H + V_{xc} + \Sigma_{DMFT} - V_{dc} = 0. \quad (13)$$

A note is in order here. We assumed  $\delta P/\delta G = 0$ , which holds whenever the projector does not depend on the self-consistent charge density. To ensure this property, we used for the localized orbitals  $|\phi\rangle = \frac{u_l(r)}{r} Y_{lm}(\hat{r})$ , where the radial wave function  $u_l(r)$  is the solution of the scalar relativistic Dirac equation on the LDA charge density (rather than self-consistent charge density). Note also that the use of the self-consistently determined Wannier functions (which depend on self-consistent charge), as is commonly used in most of the LDA+DMFT implementations [24, 29, 30], leads to non-stationary LDA+DMFT solution, and non-stationary free energies.

We next insert the expression  $G^{-1} - G_0^{-1}$  into Eq. 12 to obtain expression for free energy

$$\begin{aligned} F = & E_{nuc-nuc} - \text{Tr}((V_H + V_{xc})\rho) + E^H[\rho] + E^{xc}[\rho] \\ & + \text{Tr} \log G - \text{Tr}(\Sigma_{DMFT} G) + \Phi^{DMFT}[G_{loc}] \\ & + \text{Tr}(V_{dc}\rho_{loc}) - \Phi^{DC}[\rho_{loc}] + \mu N \end{aligned} \quad (14)$$

The impurity free energy  $F_{imp}$  contains  $\Phi^{DMFT}[G_{imp}]$  in the following way

$$F_{imp} = \text{Tr} \log G_{imp} - \text{Tr}(\Sigma_{imp} G_{imp}) + \Phi^{DMFT}[G_{imp}] \quad (15)$$

In DMFT,  $G_{loc} = G_{imp}$  and  $\Sigma_{DMFT} = \Sigma_{imp}$ , hence we can write

$$\begin{aligned} F = & E_{nuc-nuc} - \text{Tr}((V_H + V_{xc})\rho) + E^H[\rho] + E^{xc}[\rho] \\ & + \text{Tr} \log(G) - \text{Tr} \log(G_{loc}) + F_{imp} \\ & + \text{Tr}(V_{dc}\rho_{loc}) - \Phi^{DC}[\rho_{loc}] + \mu N. \end{aligned} \quad (16)$$

This equation appears as Eq.4 in the main text.

Next we split free energy of the impurity into the energy and the entropy term

$$F_{imp} = E_{imp} - TS_{imp},$$

where

$$\begin{aligned} E_{imp} = & \text{Tr}((\Delta + \varepsilon_{imp} - \omega_n \frac{d\Delta}{d\omega_n})G_{imp}) \\ & + \frac{1}{2} \text{Tr}(\Sigma_{imp} G_{imp}) - TS_{imp} \end{aligned} \quad (17)$$

Hence

$$\begin{aligned} F = & \frac{1}{2} \text{Tr}(\Sigma_{imp} G_{imp}) - \Phi^{DC}[\rho_{loc}] - TS_{imp} \\ & + E_{nuc-nuc} - \text{Tr}((V_H + V_{xc})\rho) + E^H[\rho] + E^{xc}[\rho] \\ & + \text{Tr} \log(G) - \text{Tr} \log(G_{loc}) + \text{Tr}(V_{dc}\rho_{loc}) + \mu N \\ & + \text{Tr}((\Delta + \varepsilon_{imp} - \omega_n \frac{d\Delta}{d\omega_n})G_{imp}) \end{aligned} \quad (18)$$

Again using the identity  $G_{imp} = G_{loc}$  and  $\rho_{imp} = \rho_{loc}$  as well as the definition of  $E_2$  (Eq. 10) and  $E_3$  (Eq. 11) we obtain

$$\begin{aligned} F = & \text{Tr} \log(G) + \mu N + E_2 \\ & + \text{Tr}((\Delta - \omega_n \frac{d\Delta}{d\omega_n} + \varepsilon_{imp} + V_{dc})G_{loc}) \\ & - \text{Tr} \log(G_{loc}) + E_3 - TS_{imp} \end{aligned} \quad (19)$$

This equation is implemented in our DFT+DMFT code. Similarly than in the implementation of the total energy Eq. 8, we compute  $E_3$  and  $TS_{imp}$  using impurity quantities, while the rest of the terms are computed using the Green's function of the solid. [Alternatively, we could also compute the last two rows using impurity quantities, and the first row using the solid Green's function]. In this way we ensure that  $F$  and  $E$  are split in the same way between the "impurity" and the "lattice" quantities, hence they share almost identical Monte Carlo noise. However, when comparing  $E(V)$  and  $F(V)$  at two different volumes,  $F(V)$  converges faster than  $E(V)$  with the number of LDA and/or DMFT iterations. Moreover,  $F(V)$  is very robust with respect to small changes in projector or double-counting, while  $E$  is more sensitive.

Notice that  $F + TS_{imp}$  can be evaluated at each LDA+DMFT iteration, just like the total energy above.



To add  $TS_{imp}$  at low temperatures, we however need a few extra impurity runs. The method of computing  $TS_{imp}$  is explained in the main text, and requires the impurity energy at a few temperatures. An alternative to this approach is to compute  $TS_{imp}$  from so called "flat-histogram sampling method" [54], which is also done as postprocessing on self-consistent LDA+DMFT hybridization  $\Delta$ .

Perhaps, the most challenging term in Eq. 19 to com-

pute is  $\text{Tr}\log(G)$ , which requires eigenvalues (but not eigenvectors) of the LDA+DMFT eigenvalue problem. We first diagonalize

$$\begin{aligned} (-\nabla^2 + V_{ext} + V_H + V_{xc} + \Sigma(i\omega_n) - V_{dc})\psi_{i,k,\omega_n} = \\ = \varepsilon_{i,k,\omega_n}\psi_{i,k,\omega_n}. \end{aligned} \quad (20)$$

and then evaluate

$$\text{Tr}\log(G) + \mu N = T \sum_{i\omega_n, i, k, \sigma} (\log(\varepsilon_{i,k,\omega_n} - i\omega_n - \mu) - \log(\varepsilon_{i,k,\infty} - i\omega_n - \mu)) - T \sum_{i, k, \sigma} \log(1 + e^{-\beta(\varepsilon_{i,k,\infty} - \mu)}) + \mu N \quad (21)$$

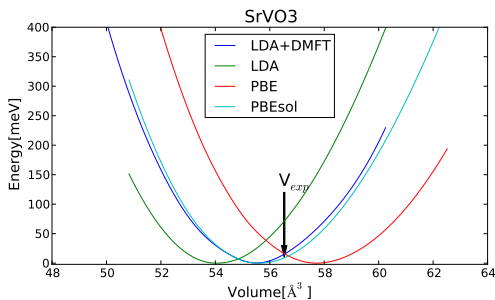


FIG. 4: Free energy of LDA+DMFT for SrVO<sub>3</sub> compared with total energy of other standard DFT functionals.

Here it becomes apparent that if  $\Sigma(i\omega_n)$  is frequency independent, the first term in the brackets vanishes, while the second term gives (at  $T = 0$ ) the sum of eigenvalues

$$\text{Tr}\log(G) + \mu N \xrightarrow{U=0} \sum_{i,k,\sigma} \theta(\varepsilon_{i,k} < \mu) \varepsilon_{i,k},$$

the well known DFT contribution to the total energy.

### COMPARISON WITH STANDARD FUNCTIONALS

Here we compare total energy of LDA, PBE [55], and PBEsol [56] functionals with the free energy of LDA+DMFT.

In most weakly correlated solids, LDA underestimates lattice constants on average for 1.6%, while PBE [55] overestimates them for approximately 1%. [2] PBEsol [56] was designed to predict most accurate volumes in solids, and it typically falls in-between LDA and PBE.

In Fig. 4 we compare LDA+DMFT free energy in SrVO<sub>3</sub> with the total energy computed by other functionals. Both LDA+DMFT and PBEsol underestimate lattice constant for approximately 0.6%, while LDA under-

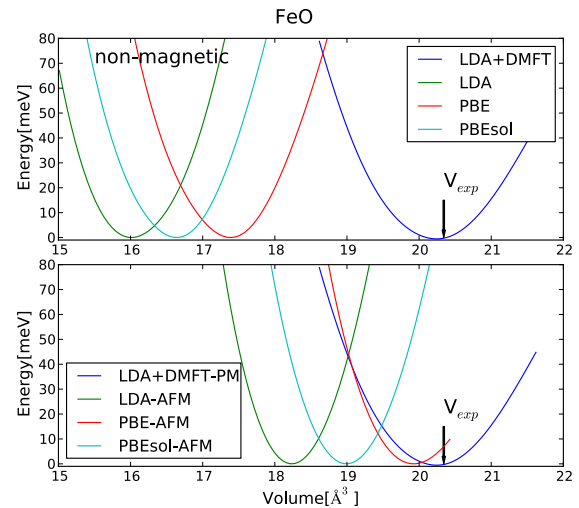


FIG. 5: Free energy of LDA+DMFT for FeO compared with total energy of other standard DFT functionals. Upper (lower) panel shows non-magnetic (antiferromagnetic) DFT calculation. LDA+DMFT results are obtained at 300K in paramagnetic state.

estimates it for 1.5%, and PBE overestimates for 0.7%. Hence predictions of standard functionals in the case of SrVO<sub>3</sub> are quite in line with standard performance in weakly correlated solids. Perhaps, this is not very surprising given that SrVO<sub>3</sub> is a metallic moderately correlated system.

In FeO (Fig. 5), all standard functionals severely underestimate volume in the paramagnetic state. For example the lattice constants with LDA, PBEsol and PBE are 7.7%, 6.5% and 5.1% too small, far outside the standard performance of these functionals in weakly correlated solids.

The predictions are improved when the AFM long range order is allowed. LDA and PBEsol still underestimate lattice constant for 3.6%, and 2.3% respectively.

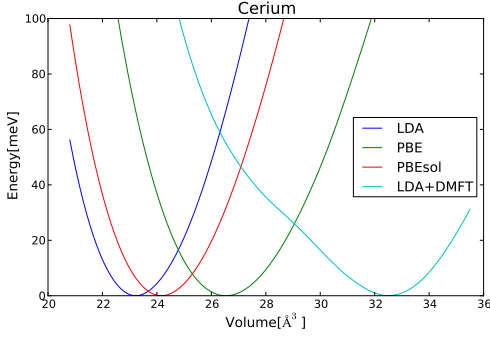


FIG. 6: Free energy of LDA+DMFT for Cerium compared with total energy of other DFT functionals. LDA+DMFT results are obtained at 400 K.

On the other hand PBE is this time quite close to the experiment (underestimates for 0.7%). In comparison LDA+DMFT underestimates it for only 0.16%. It is quite clear that the excellent prediction of AFM-PBE here is merely a coincidence, as normally PBE overestimates the volume.

Finally, we plot results for Cerium in Fig. 6. The result of LDA+DMFT is very different from those of any other functional, as it clearly contains the nontrivial soft mode for the  $\alpha$ - $\gamma$  transition. No other functional shows any hint of such transition.

The equilibrium volume in Cerium is strongly temperature dependent, and is approximately  $34\text{\AA}^3$  at zero pressure and 400 K, while it changes to approximately  $28\text{\AA}^3$  in the  $\alpha$  phase at low temperature. The LDA+DMFT results are computed at 400 K, hence at  $p = 0$  the volume is somewhat underestimated (1.5%), but under pressure (already at 1 GPa) the agreement with experiment is considerably improved.

The DFT results should be compared to  $T = 0$  experimental volume of  $28\text{\AA}^3$ . All functionals underestimate the lattice constant, LDA for 6%, PBEsol for 5% and PBE for 1.8%. Clearly electronic correlations are very important even in the  $\alpha$  phase at low temperature, as standard DFT functionals substantially underestimate the volume.

### SCREENED COULOMB REPULSION OF YUKAWA FORM

It is noted above that we used the Yukawa representation of the screened Coulomb interaction, in which there is unique relationship between the Hubbard  $U$  and Hund's coupling  $J$ . If  $U$  is specified,  $J$  is uniquely determined. To show this we derive the matrix elements of screened Coulomb interaction in our DMFT orbital basis

$$U_{m_1 m_2 m_3 m_4} = \int d^3 r \int d^3 r' \left( \frac{u_l(r)}{r} \right)^2 \left( \frac{u_l(r')}{r'} \right)^2 Y_{lm_1}^*(\hat{\mathbf{r}}) Y_{lm_2}(\hat{\mathbf{r}}) Y_{lm_3}^*(\hat{\mathbf{r}}') Y_{lm_4}(\hat{\mathbf{r}}') \frac{e^{-\lambda|\mathbf{r}-\mathbf{r}'|}}{|\mathbf{r}-\mathbf{r}'|} \quad (22)$$

There exist a well known expansion of Yukawa interaction in terms of spheric harmonics  $Y_{km}$ , which reads

$$\frac{e^{-\lambda|\mathbf{r}-\mathbf{r}'|}}{|\mathbf{r}-\mathbf{r}'|} = 4\pi \sum_k \frac{I_{k+1/2}(r_<) K_{k+1/2}(r_>)}{\sqrt{r_< r_>}} \sum_m Y_{km}^*(\hat{\mathbf{r}}) Y_{km}(\hat{\mathbf{r}}') \quad (23)$$

Here  $r_< = \min(r, r')$ ,  $r_> = \max(r, r')$ ,  $I$  and  $K$  are modified Bessel function of the first and second kind. Inserting this expression into Eq. 22, we get

$$U_{m_1 m_2 m_3 m_4} = \sum_k \frac{4\pi}{2k+1} \langle Y_{lm_1} | Y_{km_1-m_4} | Y_{lm_4} \rangle \langle Y_{lm_2} | Y_{km_3-m_2}^* | Y_{lm_3} \rangle \times (2k+1) \int_0^\infty dr \int_0^\infty dr' u_l^2(r) u_l^2(r') \frac{I_{k+1/2}(\lambda r_<) K_{k+1/2}(\lambda r_>)}{\sqrt{r_< r_>}}. \quad (24)$$

Hence, the screened Coulomb interaction has the Slater form with the Slater integrals being

$$F^k = (2k+1) \int_0^\infty dr \int_0^\infty dr' u_l^2(r) u_l^2(r') \frac{I_{k+1/2}(\lambda r_<) K_{k+1/2}(\lambda r_>)}{\sqrt{r_< r_>}}. \quad (25)$$

This is a product of two one-dimensional integrals and is very easy to efficiently implement.

It is clear from Eq. 25 that  $\lambda$  uniquely determines all  $F^k$ 's, and furthermore even one Slater integral ( $F^0$ )

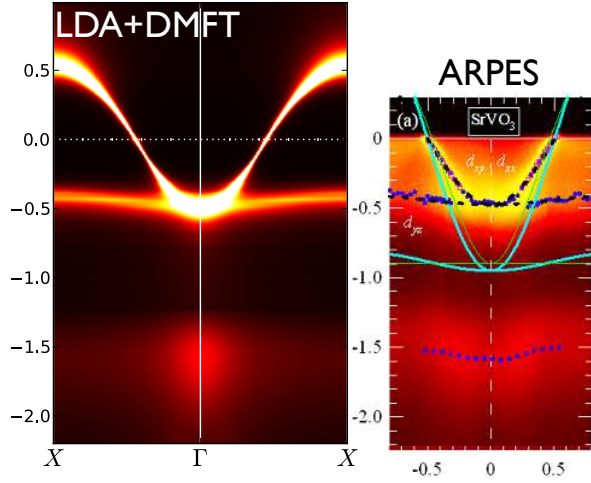


FIG. 7: Spectral function of  $\text{SrVO}_3$  within LDA+DMFT at equilibrium volume compared with ARPES spectra of Ref. 57.

uniquely determines  $\lambda$ . This is because  $F^k$  are monotonic functions of  $\lambda$  and take the value of bare  $F^k$  at  $\lambda = 0$  and vanish at large  $\lambda$ . Hence given  $F^0$ , the screening length

$\lambda$  is uniquely determined, and hence other higher order  $F^k$  are uniquely determined as well.

### MASS RENORMALIZATION OF METALLIC $\text{SrVO}_3$

Even though the Coulomb interaction in  $\text{SrVO}_3$  is  $U = 10$  eV, it gives a relatively moderate mass enhancement over DFT band structure in all-electron LDA+DMFT implementation. This is because the interaction is severely screened by hybridization of  $d$  states with oxygen  $p$  states, and because the  $t_{2g}$  orbitals are in mixed-valence state ( $n_{t_{2g}} \approx 1.5$ ) [39, 40]. In Fig. 7 we show the LDA+DMFT spectral function as well as recent ARPES measurements [57]. The mass renormalization in the  $t_{2g}$  orbital is  $m_{t_{2g}}^*/m_{band} \approx 2$  and in  $e_g$  is  $m_{t_{2g}}^*/m_{band} \approx 1.3$ . The agreement between ARPES spectra (the experimental signal is color coded on the right) and LDA+DMFT spectral function  $A(k, \omega)$  (plotted on the left) is very good, both in the quasiparticle band (between  $-0.5$  eV and  $0.5$  eV) and Hubbard satellite at  $-1.5$  eV.